Propagation dynamics of optically generated unipolar electromagnetic pulses

S. A. Sychugin, A. L. Novokovskaya, and M. I. Bakunov*
Department of Radiophysics, University of Nizhny Novgorod, Nizhny Novgorod 603022, Russia

(Received 19 January 2022; accepted 12 May 2022; published 31 May 2022)

It was recently predicted [M. I. Bakunov, A. V. Maslov, and M. V. Tsarev, Phys. Rev. A **95**, 063817 (2017)] that an ultrashort laser pulse producing multiphoton ionization in an electro-optic crystal can generate a quasistatic unipolar electromagnetic precursor propagating ahead of the laser pulse. Here we study the propagation dynamics of such a precursor outside the generating crystal. Our analysis is based on a specially developed semianalytical model that represents the precursor generation as radiation from sequentially switched discrete current-carrying ribbons distributed along the laser path. The model allows for calculating the precursor spatiotemporal structure at an arbitrarily long distance behind the crystal. The calculations reveal the complex propagation dynamics of the precursor. Starting as a unipolar pulse, it becomes quasiunipolar after some distance, which depends on the precursor transverse size, and then bipolar preserving a constant transverse size and maximum field strength. These findings are important for the experimental observation of the precursors and their practical use.

DOI: 10.1103/PhysRevA.105.053528

I. INTRODUCTION

Strong unipolar and quasiunipolar electromagnetic pulses are a subject of current interest due to their potential for new regimes of light-matter interaction [1]. In particular, unipolar (half-cycle) terahertz pulses can be more efficient, compared to the standard bipolar and few-cycle pulses, for ultrafast control of the Rydberg atom dynamics [2] and femtochemistry on metal surfaces [3], molecular orientation and alignment [4,5], nonlinear terahertz spectroscopy [6], particle acceleration [7,8], and terahertz streaking [9].

The unipolar terahertz pulses can be generated in the near-field region of photoconductive switches [10] and laser-driven plasma in solid targets [11]. One-cycle pulses can be converted into unipolar pulses by reflection from a thin layer of a linear medium [12]. More sophisticated methods of producing stronger unipolar pulses by nonuniform amplification of one-cycle pulses in nonequilibrium fast relaxing plasma [13] and by spatial phase modulation of terahertz pulses optically generated in a layer of resonant nonlinear medium [14] have been discussed.

Recently [15], it was found that high-field unipolar pulses can be generated by femtosecond laser pulses propagating in electro-optic crystals in the regime of high optical intensity, when the laser pulse experiences optical rectification and simultaneously produces multiphoton ionization in the crystal. In this regime, photogenerated carriers are accelerated by the electric field copropagating the nonlinear polarization induced by the laser pulse in the crystal. This creates a current surge, which in turn generates electromagnetic fields. The process is repeated continuously along the laser propagation distance. In materials with $n_g > n_0$, where n_g is the optical group refractive index and n_0 is the low-frequency phase refractive index, the generated low-frequency fields propagate faster than the laser pulse and form a quasistatic electromagnetic precursor ahead of the laser pulse. The unipolar electric and magnetic fields in the precursor generated by a Ti:sapphire laser pulse in GaP or ZnTe can exceed the terahertz fields behind the laser pulse [15,16]. In materials with $n_g < n_0$, such as $LiNbO_3$, the generation of unipolar precursors with the electric and magnetic fields as strong as hundreds of kV/cm and thousands of gauss by laser pulses with a tilted pulse front was predicted [17].

To observe the quasistatic unipolar precursors experimentally and use them practically, the usual terahertz schemes with focusing optics are inapplicable. The electric field in the focus is proportional to the time derivative of the incident field and therefore focusing destroys unipolarity. Even without focusing optics, how long the precursor can preserve unipolarity upon exiting the crystal is an open question. Indeed, propagation from the near field to the far field leads to reshaping effects [10,18]. Since the precursor has a broad spectrum, which starts from zero frequency, a given distance can be in the near field for the high frequencies and in the far field for the lower ones. Moreover, for the dc component with the wavelength $\lambda \to \infty$ there is no near-field region in terms of the Fraunhofer distance $L_F \sim d^2/\lambda$ (d is the transverse size of the precursor). All this implies a complicated dynamics of the precursor propagation in free space behind the generator crystal [19]. (The propagation of unipolar pulses in coaxial waveguides was considered in Ref. [20].)

In Ref. [16], two-dimensional (2D) numerical calculations using the finite-difference time-domain (FDTD) method were carried out to model the propagation of a precursor generated by a Ti:sapphire laser in a 3-mm-thick GaP crystal. The calculations were limited to a 2-mm distance in free space behind the crystal and showed that the precursor preserves its unipolar waveform at this distance. Due to inherent limitations

*bakunov@rf.unn.ru

of FDTD modeling, such calculations cannot be made for substantially longer distances.

In this paper, we develop a semianalytical 2D model that represents the precursor generation as a radiation from sequentially switched discrete current-carrying ribbons distributed along the laser path. Since the radiation fields of the ribbons are written analytically, they can be numerically summarized at an arbitrarily long distance behind the crystal. Thus, the model allows for calculating the long-distance dynamics of the precursor propagation in free space.

The results of our calculations show that the quasistatic precursor of a several-millimeter transverse size can propagate a few centimeters as a unipolar and then quasiunipolar field structure. After that the precursor propagates a few tens of centimeters as a bipolar field structure of a constant transverse size and with the field peaks of a constant amplitude which are sharpening with distance. Finally, the peaks start to decline, indicating the onset of the far-field regime.

II. MODEL

Let a pump laser pulse propagate with the optical group velocity $V = c/n_g$ (c is the speed of light) in an electro-optic crystal of thickness L_c. We take the z axis along the propagation direction. The laser beam is assumed to have a finite width in the x direction and be infinite in the y direction. This 2D approximation is relevant to the case of focusing the beam to a line by a cylindrical lens, the geometry often used in the terahertz generation schemes [21,22]. The laser pulse induces a nonlinear polarization in the crystal via nonlinear optical rectification. The polarization direction is determined by the laser pulse polarization and crystallographic orientation of the crystal. We assume that the nonlinear polarization is along the y axis and therefore it generates the electric and magnetic fields with the components E_y and B_x, B_z, respectively. The electric field creates a surge current of photogenerated carriers in the y direction, which acts as a source of a quasistatic precursor [15].

We model the continuous generation of the precursor in the crystal by emission of electromagnetic fields from a set of N discrete current-carrying ribbons ($-d/2 < x < d/2$) uniformly distributed with period Δz in the interval $0 < z < L_c$ (Fig. 1). The ribbon width d models the transverse size of the laser pulse. Currents on the ribbons are sequentially switched on by the front moving with the optical group velocity V, kept constant for a time T, which models the laser pulse duration, and then switched off. Thus, the current density on the ith ribbon is written as

$$j_i = J[\eta(t - t_i) - \eta(t - t_i - T)]\delta(z - z_i), \tag{1}$$

where J is the current density magnitude, $\eta(t)$ is the Heaviside unit function, $\delta(z)$ is the Dirac delta function, $z_i = i\Delta z$, $t_i = z_i/V$, and $i = 0, 1, \ldots, N-1$. Equation (1) implies that the laser pulse duration T is much smaller than the photoexcited carrier lifetime, similarly to Refs. [15–17]. The electron-hole recombination in semiconductors occurs typically on the nanosecond timescale [23,24] and therefore can be safely neglected for femtosecond excitation.

The electric and magnetic fields created by a ribbon can be found analytically. For clarity, we derive below only the electric field created by the ribbon placed at $z = 0$ (i.e., with $i = 0$). The generalization for a ribbon at $z_i \neq 0$ is straightforward. Also, we describe the dynamics of the electric field formation only after switching on the current on the ribbon. The switching off of the current is equivalent to the switching on of the oppositely directed current [Eq. (1)] and therefore leads to the same dynamics of the electric field of the opposite sign.

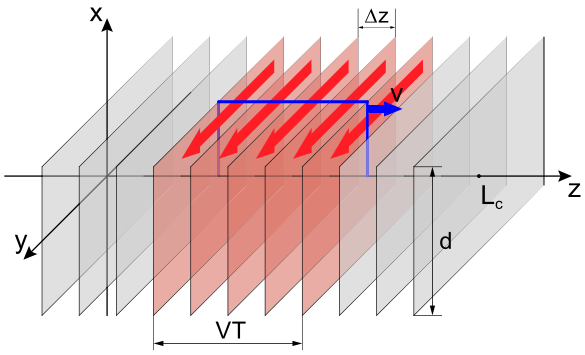

FIG. 1. Discrete model of the precursor source. Currents (red arrows) on the ribbons are switched on by the front moving with the optical group velocity V, kept constant for a time T, and then switched off.

By using the Green's function of the 2D wave equation [25]

$$G(R, \tau) = -\frac{v}{2\pi}\frac{\eta(v\tau - R)}{\sqrt{v^2\tau^2 - R^2}}, \tag{2}$$

where $\tau = t - t'$, $R = [(x - x')^2 + z^2]^{1/2}$, and $v = c/n_0$ is the phase velocity of the low-frequency waves in the crystal, we write the solution of the wave equation for the single y component of the vector potential as

$$A_y(x, z, t) = \frac{2J}{n_0}\int_{-d/2}^{d/2} dx' \int_0^{t-R/v} dt' \frac{\eta(vt - R)}{\sqrt{v^2\tau^2 - R^2}}. \tag{3}$$

Performing the integral over t', we obtain

$$A_y = \frac{2J}{c}\int_{-d/2}^{d/2} dx' \eta(vt - R) \ln\frac{vt + \sqrt{v^2t^2 - R^2}}{R}. \tag{4}$$

Finally, by using the relation $E_y = -(1/c)\partial A_y/\partial t$, we obtain following formulas for the electric field in three specific time-spatial regions (due to bilateral symmetry about the y-z plane the formulas are given only for $x \geqslant 0$):

$$E_y = -\frac{2J}{cn_0}\pi \tag{5}$$

for $\sqrt{v^2t^2 - z^2} < d/2 - x$ [region I in Figs. 2(a) and 2(b)],

$$E_y = -\frac{2J}{cn_0}\left(\frac{\pi}{2} + \arcsin\frac{d/2 - x}{\sqrt{v^2t^2 - z^2}}\right) \tag{6}$$

for $|d/2 - x| < \sqrt{v^2t^2 - z^2} < d/2 + x$ [region II in Figs. 2(a) and 2(b)], and

$$E_y = -\frac{2J}{cn_0}\left(\arcsin\frac{d/2 + x}{\sqrt{v^2t^2 - z^2}} + \arcsin\frac{d/2 - x}{\sqrt{v^2t^2 - z^2}}\right) \tag{7}$$

for $\sqrt{v^2t^2 - z^2} > d/2 + x$ [region III in Fig. 2(b)].

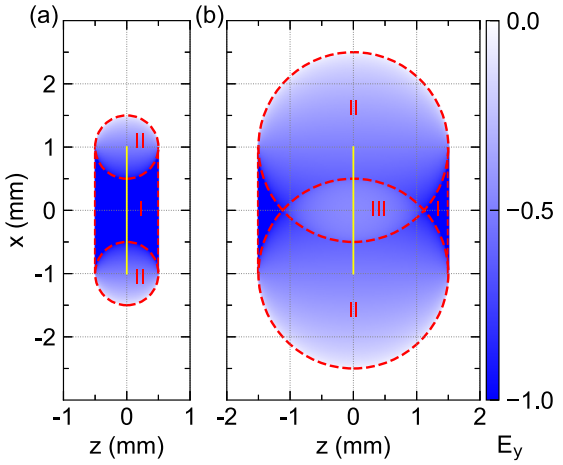

FIG. 2. Snapshots of the electric field E_y (normalized to $2\pi J/cn_0$) emitted by the ribbon current with $d = 2$ mm placed at $z = 0$ for two moments of time (a) $t = d/4v$ and (b) $t = 3d/4v$ after the switching on of the current at $t = 0$. Regions I, II, and III correspond to Eqs. (5), (6), and (7), respectively [with the change $x \to -x$ in Eq. (6) for $x < 0$].

It can be seen from Fig. 2(a) that switching on the current on the ribbon gives rise to the emission of constant electric and magnetic (not shown in Fig. 2) fields that propagate in both $\pm z$ directions (region I). The generation of a magnetic field by current seems natural; the concurrent generation of an electric field can be explained by the necessity of a nonzero energy flow from the source.

The fields in region I are a germ of the quasistatic precursor formed by the sequence of switching on current ribbons. The front of the constant fields propagates with the velocity v, which exceeds the velocity V of the front that switches on currents on the ribbons. Therefore, the constant fields from a sequence of ribbons propagate ahead of the switching front and form a precursor that propagates in the $+z$ direction. The constant fields emitted in the $-z$ direction should be neglected because in practice plasma behind the laser pulse prohibits the fields from penetrating into the plasma region.

An infinitely wide current ribbon, i.e., a current plane, would generate an expanding region I with constant fields for infinite time. Due to the finite width of the ribbon, two cylindrical regions [regions II in Fig. 2(a)], where E_y is given by Eq. (6) and weaker than in region I, also start to propagate from the ribbon ends $x = \pm d/2$ at $t = 0$. As a result, region I of strong constant fields shrinks with time in the x direction [Fig. 2(a)]. For $t > d/2v$, two regions II intersect and form region III, which separates region I from the current ribbon [Fig. 2(b)]. From this moment, the region of constant fields propagates independently of the source as a kind of unipolar electromagnetic bullet [19,26]. The transverse (along the x axis) size of the bullet equals d and does not change in the course of propagation. The longitudinal (along the z axis) size of the bullet decreases as $\sim 1/z$ for $z \gg d/2$. The maximum electric and magnetic fields in the bullet preserve their values.

Returning to the problem of calculating the total electric field from the set of N current ribbons sequentially switched on and off [Eq. (1)], we represent the total field at an observation point as a sum

$$E_y(x,z,t) = \sum_{i=0}^{N-1} [E_{yi}(x, z - z_i, t - t_i) - E_{yi}(x, z - z_i, t - t_i - T)], \quad (8)$$

where the contributions E_{yi} from the ith current ribbon are taken in the form of Eq. (5), (6), or (7) according to the above-given conditions of their existence (with changes $z \to z_i$ and $t \to t - t_i$ or $t \to t - t_i - T$). Thus, the total field at an observation point is in general a superposition of partial (from individual ribbons) fields, which correspond to different propagation regions (I, II, and III) and can be of different signs due to opposite signs of the terms on the right-hand side of Eq. (8). This determines a complex spatiotemporal dynamics of the total field. To calculate the field outside the crystal, we set $n_0 = 1$ in Eqs. (5)–(7).

III. RESULTS AND DISCUSSION

To verify the correctness of the approach developed in Sec. II, we apply it first to calculate the precursor formation in the crystal and compare our results with the results of accurate FDTD calculations [16]. We use the same refractive indices $n_g = 3.66$ and $n_0 = 3.31$, which correspond to a GaP crystal excited by a Ti:sapphire laser, and the same crystal thickness $L_c = 3$ mm as in Ref. [16]. In the calculations below, the total number of ribbons is $N = 3000$ ($\Delta z = 1$ μm) and the number of ribbons within the current pulse length VT ($T = 250$ fs) is 20. The discretization step ($\Delta z = 1$ μm) is sufficiently small to obtain smooth (with negligible discretization effects) field distributions, which are practically not improved by a further decrease of Δz (increase of N).

Figure 3 shows the dynamics of the precursor formation for two ribbon widths $d = 8$ and 2 mm. The precursor is formed as a pulse of negative polarity just before the front that switches on current ribbons. The transverse size of the precursor does not change and equals the ribbon width [Figs. 3(a) and 3(b)]. The length of the precursor grows monotonically in the crystal with the velocity $v - V$ due to accumulation of the fields emitted by different ribbons. This dynamics agrees well with the results of FDTD calculations [16].

Despite the similar formation dynamics, the structure of the precursors in Figs. 3(a) and 3(b) differs substantially. For $d = 8$ mm, the field is distributed uniformly over the precursor in both the transverse and longitudinal directions [Figs. 3(a) and 3(c)]. The precursor exhibits a distinct unipolar character [1]. For $d = 2$ mm, regions of a stronger and a weaker field in the precursor can be seen [Fig. 3(b)] and the field on the axis decreases to the end of the precursor [Fig. 3(c)]. There is also a weak long tail of opposite (positive) polarity behind the precursor, i.e., the precursor constitutes a part of a quasiunipolarlike pulse [1]. These results also agree with Ref. [16], where the generation of a well-formed plateaulike precursor was predicted for the laser transverse size (full width at half maximum) larger than ~3.5–5 mm and a decrease in the precursor field was predicted for smaller laser sizes.

Now let us apply the developed method to calculating the propagation dynamics of the precursor in free space behind

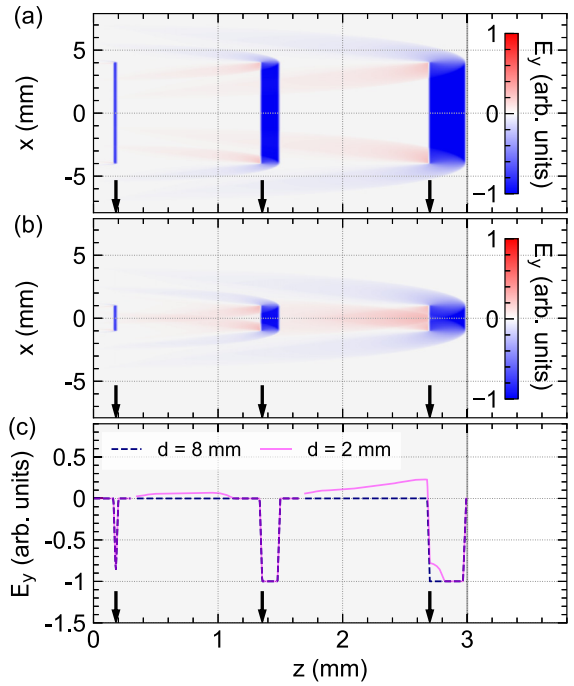

FIG. 3. Snapshots of E_y (normalized to the maximum value) at three moments of time for (a) $d = 8$ mm and (b) $d = 2$ mm. (c) Snapshots of E_y on the z axis (at $x = 0$) for the same values of d. The current pulse duration is $T = 250$ fs. The arrows indicate the position of the front moving with the velocity V inside the crystal (shaded region $0 < z < 3$ mm).

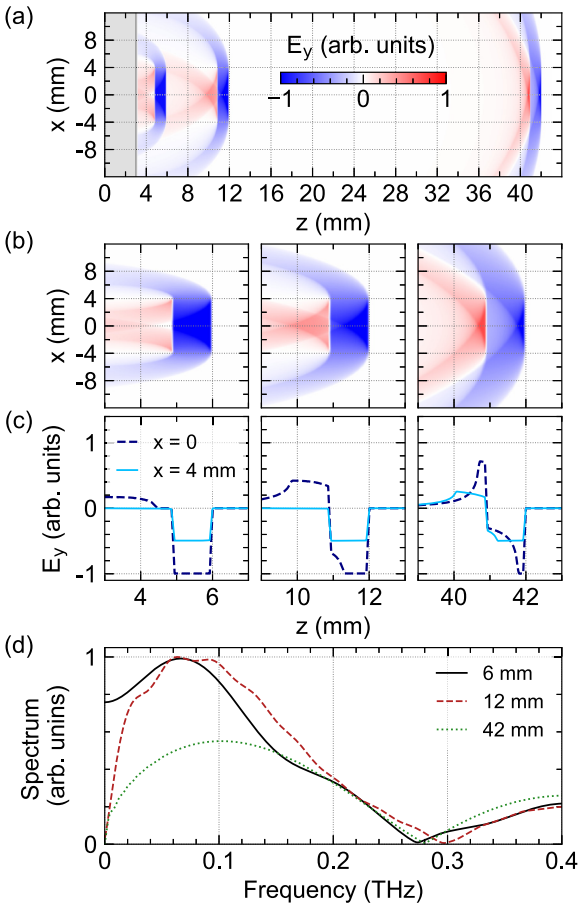

FIG. 4. (a) and (b) Snapshots of E_y (normalized to the maximum value) at three moments of time for $d = 8$ mm and $T = 250$ fs. (c) Snapshots of E_y at $x = 0$ and $x = d/2$ for the same moments of time. (d) Spectra of the fields at $x = 0$ for the same moments of time. In (a) the shaded region ($0 < z < 3$ mm) shows the crystal.

the generating crystal ($z > L_c$, $L_c = 3$ mm). We will consider the precursor generated by the ribbons with $d = 8$ mm. This width is sufficient for generating a well-formed unipolar precursor at the crystal exit boundary [Fig. 3(a)]. For the calculations, we set $n_0 = 1$ and $n_g = 1.35$ in the formulas of Sec. II. The value of n_g is determined from the condition of a correct precursor length in free space, which is 3.66 times longer than in the crystal.

Figure 4(a) shows the snapshots of the electric field E_y at three moments of time, when the precursor is at the distances $z - L_c$ of 3, 9, and 39 mm from the crystal exit boundary ($z = L_c = 3$ mm). The field structure of the precursor at these distances is shown in more detail in Figs. 4(b) and 4(c). After propagating about 3 mm, the region of a strong field narrows in its rear part and becomes almost triangular [compare Fig. 4(b), left panel, with Fig. 3(a)] but the field itself remains uniform in this region and of the same strength as at the crystal boundary. Despite the appearance of a weak tail in the waveform at $x = 0$, the waveforms at both $x = 0$ and $x = d/2 = 4$ mm preserve their unipolar character [Fig. 4(c), left panel]. This is confirmed by the waveform ($x = 0$) spectrum which has a nonzero spectral amplitude at zero frequency [Fig. 4(d)]. Thus, at the distances $z - L_c \lesssim 3$ mm the precursor propagates as a unipolar electromagnetic pulse.

For $z - L_c \gtrsim 3$ mm, the triangular region of a strong field starts shrinking in the longitudinal (along the z axis) direction and acquires a swallow-tail shape [Fig. 4(b), middle panel]. Simultaneously, the tail of the field of opposite polarity becomes stronger and shorter. As a result, the waveform at $x = 0$ [Fig. 4(c), middle panel] acquires a typical quasiunipolar shape with a short leading half-cycle part and a long weak tail of opposite polarity [1]. The negligible spectral amplitude at zero frequency [Fig. 4(d)] indicates a close to zero electric field area of the waveform [1]. Interestingly, the waveform at $x = d/2 = 4$ mm preserves a unipolar character. The transverse size of the high-field region and the field strength in the region remain the same as at the crystal boundary. Such spatiotemporal field structure can be called a quasiunipolar electromagnetic bullet. This propagation regime continues up to distances as long as $z - L_c \sim 40$ mm. In practice, the quasiunipolar pulses can be used to control nonlinear systems in a similar way to the unipolar pulses [27].

At the distances $z - L_c \sim 40$ mm, the waveform at $x = 0$ approaches the time derivative of the rectangularlike waveform at the exit crystal boundary, i.e., acquires two sharp peaks of opposite polarity in the beginning and in the end [Fig. 4(c), right panel]. The low-frequency part of the spectrum is depleted by diffraction [Fig. 4(d)]. The transverse size of the high-field regions and the field strength in the regions are still the same as at the crystal boundary [Fig. 4(b), right panel]. Such a spatiotemporal field structure can be called a bipolar electromagnetic bullet. The precursor propagates

as a bipolar bullet up to distances as long as $z \sim 200$ mm, experiencing a sharpening of the field peaks (not shown). At distances $z \gtrsim 200$ mm, the peaks start to decline, indicating a transition to the far-field propagation regime.

IV. CONCLUSION

We developed a semianalytical model that allows for calculating the arbitrarily long-distance propagation of the quasiconstant unipolar electromagnetic fields generated by ultrashort laser pulses in electro-optic crystals in the regime of multiphoton ionization. By using the developed approach, we found that the generated unipolar fields demonstrate a complex propagation dynamics in free space behind the generating crystal. Starting propagation as a unipolar electromagnetic pulse, it gradually transforms to a quasiunipolar (with a short half-cycle leading part and a long weak tail of opposite polarity) pulse and then to a bipolar (one-cycle) pulse. Both the transverse (with respect to the propagation direction) size of the pulse and the field strength in the pulse remain the same as at the crystal boundary. Such a stable spatiotemporal field structure can be considered as a kind of electromagnetic bullet.

In particular, for a bullet with an 8 mm width the regimes of unipolar, quasiunipolar, and bipolar propagation occur at distances of $\lesssim$3 mm, ∼3–40 mm, and ∼40–200 mm, respectively. At larger distances, the bipolar field peaks start to decline, indicating the onset of the far-field propagation regime.

Since the standard terahertz detection schemes with focusing optics destroy unipolarity, the predicted propagation dynamics of unipolar and quasiunipolar electromagnetic fields is important for their experimental observation and practical use.

ACKNOWLEDGMENT

This work was supported by the Ministry of Science and Higher Education of the Russian Federation (Grant No. 075-15-2020-927).

[1] R. M. Arkhipov, M. V. Arkhipov, and N. N. Rosanov, Unipolar light: Existence, generation, propagation, and impact on microobjects, Quantum Electron. **50**, 801 (2020).

[2] A. Wetzels, A. Gürtler, L. D. Noordam, F. Robicheaux, C. Dinu, H. G. Muller, M. J. J. Vrakking, and W. J. van der Zande, Rydberg State Ionization by Half-Cycle-Pulse Excitation: Strong Kicks Create Slow Electrons, Phys. Rev. Lett. **89**, 273003 (2002).

[3] P. Salén, M. Basini, S. Bonetti, J. Hebling, M. Krasilnikov, A. Y. Nikitin, G. Shamuilov, Z. Tibai, V. Zhaunerchyk, and V. Goryashko, Matter manipulation with extreme terahertz light: Progress in the enabling THz technology, Phys. Rep. **836–837**, 1 (2019).

[4] S. Fleischer, Y. Zhou, R. W. Field, and K. A. Nelson, Molecular Orientation and Alignment by Intense Single-Cycle THz Pulses, Phys. Rev. Lett. **107**, 163603 (2011).

[5] M. Sajadi, M. Wolf, and T. Kampfrath, Transient birefringence of liquids induced by terahertz electric-field torque on permanent molecular dipoles, Nat. Commun. **8**, 14963 (2017).

[6] X. Chai, X. Ropagnol, S. M. Raeis-Zadeh, M. Reid, S. Safavi-Naeini, and T. Ozaki, Subcycle Terahertz Nonlinear Optics, Phys. Rev. Lett. **121**, 143901 (2018).

[7] W. R. Huang, E. A. Nanni, K. Ravi, K.-H. Hong, A. Fallahi, L. J. Wong, P. D. Keathley, L. E. Zapata, and F. X. Kärtner, Toward a terahertz-driven electron gun, Sci. Rep. **5**, 14899 (2015).

[8] D. Zhang, A. Fallahi, M. Hemmer, H. Ye, M. Fakhari, Y. Hua, H. Cankaya, A.-L. Calendron, L. E. Zapata, N. H. Matlis, and F. X. Kärtner, Femtosecond phase control in high-field terahertz-driven ultrafast electron sources, Optica **6**, 872 (2019).

[9] D. Zhang, A. Fallahi, M. Hemmer, X. Wu, M. Fakhari, Y. Hua, H. Cankaya, A.-L. Calendron, L. E. Zapata, N. H. Matlis, and F. X. Kärtner, Segmented terahertz electron accelerator and manipulator (STEAM), Nat. Photon. **12**, 336 (2018).

[10] K. Reimann, Table-top sources of ultrashort THz pulses, Rep. Prog. Phys. **70**, 1597 (2007).

[11] Y. Gao, T. Drake, Z. Chen, and M. F. DeCamp, Half-cycle-pulse terahertz emission from an ultrafast laser plasma in a solid target, Opt. Lett. **33**, 2776 (2008).

[12] M. V. Arkhipov, R. M. Arkhipov, A. V. Pakhomov, I. V. Babushkin, A. Demircan, U. Morgner, and N. N. Rosanov, Generation of unipolar half-cycle pulses via unusual reflection of a single-cycle pulse from an optically thin metallic or dielectric layer, Opt. Lett. **42**, 2189 (2017).

[13] A. V. Bogatskaya, E. A. Volkova, and A. M. Popov, Unipolar terahertz pulse formation in a nonequilibrium plasma channel formed by an ultrashort uv laser pulse, Phys. Rev. E **104**, 025202 (2021).

[14] A. V. Pakhomov, R. M. Arkhipov, M. V. Arkhipov, A. Demircan, U. Morgner, N. N. Rosanov, and I. Babushkin, Unusual terahertz waveforms from a resonant medium controlled by diffractive optical elements, Sci. Rep. **9**, 7444 (2019).

[15] M. I. Bakunov, A. V. Maslov, and M. V. Tsarev, Optically generated terahertz pulses with strong quasistatic precursors, Phys. Rev. A **95**, 063817 (2017).

[16] E. S. Efimenko, S. A. Sychugin, M. V. Tsarev, and M. I. Bakunov, Quasistatic precursors of ultrashort laser pulses in electro-optic crystals, Phys. Rev. A **98**, 013842 (2018).

[17] M. V. Tsarev and M. I. Bakunov, Tilted-pulse-front excitation of strong quasistatic precursors, Opt. Express **27**, 5154 (2019).

[18] D. Côté, J. E. Sipe, and H. M. van Driel, Simple method for calculating the propagation of terahertz radiation in experimental geometries, J. Opt. Soc. Am. B **20**, 1374 (2003).

[19] T. T. Wu, Electromagnetic missiles, J. Appl. Phys. **57**, 2370 (1985).

[20] N. N. Rosanov, Transportation of extremely short radiation pulses in a waveguide with a nonsimply connected cross section, Opt. Spectrosc. **127**, 1050 (2019).

[21] A. G. Stepanov, J. Hebling, and J. Kuhl, THz generation via optical rectification with ultrashort laser pulse focused to a line, Appl. Phys. B **81**, 23 (2005).

[22] S. B. Bodrov, I. E. Ilyakov, B. V. Shishkin, and M. I. Bakunov, Highly efficient Cherenkov-type terahertz generation by 2-μm wavelength ultrashort laser pulses in a prism-coupled $LiNbO_3$ layer, Opt. Express **27**, 36059 (2019).

[23] V. I. Berezhiani, S. M. Mahajan, and I. G. Murusidze, Photon accelerator: Large blueshifting of femtosecond pulses in semiconductors, Phys. Rev. A **56**, 5147 (1997).

[24] A. Wincukiewicz, W. Mech, S. Grankowska, A. Wolos, A. Drabinska, T. Slupinski, K. P. Korona, and M. Kaminska, Radiative recombination and other processes related to excess charge carriers, decisive for efficient performance of electronic devices, Lith. J. Phys. **58**, 49 (2018).

[25] P. M. Morse and H. Feshbach, *Methods of Theoretical Physics* (McGraw-Hill, New York, 1953), Chap. 7.

[26] B. Hafizi and P. Sprangle, Diffraction effects in directed radiation beams, J. Opt. Soc. Am. A **8**, 705 (1991).

[27] R. V. Arkhipov, A. Pakhomov, M. Arkhipov, A. Demircan, U. Morgner, N. N. Rosanov, and I. Babushkin, Selective ultrafast control of multi-level quantum systems by subcycle and unipolar pulses, Opt. Express **28**, 17020 (2020).